Journal of Statistical Physics, Vol. 48, Nos. 5/6, 1987

Self-Consistent Monte Carlo Simulations of the Electron and Ion Distributions of Inhomogeneous Liquid Alkali Metals. II. Longitudinal and Transverse Density Distributions in the Liquid–Vapor Interface of Binary Metallic Alloys

Jonathan G. Harris,[1] Jan Gryko,[1,2] and Stuart A. Rice[1]

Received February 24, 1987

We present the results of Monte Carlo simulations of the liquid–vapor interface of sodium–cesium alloys. The longitudinal density profile of each alloy shows that the liquid–vapor interface consists of a well-defined monolayer of cesium sitting on top of a slab of the bulk alloy. Underneath the monolayer there is a slight excess of sodium. A comparison with a van der Waals analog of one of the alloys shows that the presence of the well-defined monolayer of cesium on the outside of the liquid–vapor interface is a feature peculiar to metallic mixtures. The transverse pair correlation functions of the cesium monolayer are insensitive to the composition of the bulk of the slab.

KEY WORDS: Liquid metals; liquid–vapor interface; surface segregation; quantum statistical mechanics; Monte Carlo simulations; inhomogeneous liquids; alloys.

1. INTRODUCTION

Experimental studies and Monte Carlo simulations have established that the structure of the liquid–vapor interface of a simple metal is significantly different from that of a Lennard-Jones system. In the latter, the density along the normal through the interface (the longitudinal density distribution) monotonically decreases from the liquid to the vapor side of the

[1] Department of Chemistry and James Franck Institute, University of Chicago, Chicago, Illinois 60637.

[2] Present Address: Institute of Physical Chemistry, 01-223 Warsaw, Poland.

0022-4715/87/0900-1109$05.00/0

interface; near the triple point of the system this variation in density occurs over a range of two to three atomic diameters.[1] In the former, the longitudinal density distribution shows stratification on the liquid side of the interface and decreases rapidly, within a fraction of an atomic diameter, to the gas density on the vapor side of the interface.[2-4] The differences between the structures of the liquid–vapor interfaces of the simple metal and the Lennard-Jones fluid can be traced to the different forms of the interatomic potential energy functions. The potential energy of a Lennard-Jones system is rather accurately represented as a sum of density-independent pair interactions. In contrast, the potential energy of a metal is strongly density-dependent. In the pseudopotential representation the potential energy of a metal has two terms: a sum of pair interactions and a one-body potential, both of which are density-dependent. It is the variation with electron density of the one-body potential that is most important. In a homogeneous liquid metal the one-body potential is constant everywhere and dominates the binding energy of the system. In an inhomogeneous system, such as the liquid–vapor interface, the variation in density forces a variation in the one-body potential which acts as force constraining the ions to remain in the region where the density is high. That is, the variation through the liquid–vapor interface of the one-body potential in the pseudopotential for the metal is equivalent to the presence of a relatively steep continuous wall. It is the packing of the rest of the liquid against this wall that generates the stratification of the density in the liquid–vapor interface.

The first Monte Carlo simulations of the liquid–vapor interface of a metal, by D'Evelyn and Rice,[2] assumed that the system pseudopotential could be calculated as if the electron and smoothed ion distributions in the interface were coincident, i.e., that electroneutrality prevails at each point in the inteface. This approximation is suggested by the results of the self-consistent jellium calculations of Allen and Rice.[5] In a more recent paper, which we shall refer to as I,[4] we generalized the D'Evelyn–Rice procedure so that the electronic structure, and hence the system pseudopotential, is treated more accurately. In particular, we replaced the local electroneutrality approximation of earlier works with a density functional theory treatment of the electron gas and solved the self-consistent Kohn–Sham equations to determine the electron distribution at a jellium (smoothed ion distribution)–vacuum (vapor) interface. A comparison of the results of simulations carried out with and without the local electroneutrality assumption shows that the stratification of the interface is rather insensitive to the treatment of the electronic structure.

Given that the one-body term in the pseudopotential plays the dominant role in defining the longitudinal density distribution in the

liquid–vapor interface, it is reasonable to expect it to play a role in defining the extent of composition segregation at the surface of a binary alloy. In the present work we attempt to answer three questions:

1. How does the longitudinal density distribution in the liquid–vapor interface vary among alloys of different composition?
2. Which features of the longitudinal density distribution in the liquid–vapor interface of an alloy are attributable to effects associated with the different ion core sizes and which to effects associated with the variation of the one-body term in the potential energy?
3. How does the transverse pair correlation function in the liquid–vapor interface vary with the composition and longitudinal density distribution in the interface?

The vehicle for our analysis of the structure and composition of the liquid–vapor interface of an alloy is Monte Carlo simulation of the system. We report the results of Monte Carlo simulations of the liquid–vapor interfaces of several NaCs alloys using the self-consistent pseudopotential methodology of Harris, Gryko, and Rice. Our new results, which greatly extend the earlier work of Gryko and Rice,[6] show the following.

1. In the NaCs system, Cs concentrates at the liquid–vapor interface, as predicted by thermodynamic arguments. In the alloys we have studied, the outermost layer of the liquid–vapor interface is essentially pure Cs.

2. The variation of composition with position in the interface is very different in metallic and van der Waals mixtures. In the NaCs alloys we have simulated, the Cs that segregates at the surface sits atop a layer slightly depleted in Cs, and underneath this layer the bulk composition is achieved. Put another way, the interface concentration is different from the bulk concentration for only about one atomic diameter into the bulk liquid. In the model van der Waals system generated by turning off the one-body potential in the pseudopotential, the extent of composition segregation is less than when the one-body potential is nonzero and, more important, the interface concentration is different from the bulk concentration for about five atomic diameters into the bulk liquid.

3. The transverse pair correlation function in the outermost layer of the liquid–vapor interface, which is pure cesium, does not depend on the bulk composition of the alloy and is identical to the transverse pair correlation function in the outermost peak of the liquid–vapor interface of pure Cs.

2. THE SYSTEM HAMILTONIAN

The Hamiltonian for the inhomogeneous binary alloy is very similar to that of the pure liquid metal except that the pair potential and the one-body potential (the structure-independent term) depend on both the positions of the ions and their types. We use the generalization of the D'Evelyn–Rice Hamiltonian[2]

$$\mathbf{H} = \sum_i \frac{p_i^2}{2m_i} + U_0[\rho_0(\mathbf{r}), n_e(\mathbf{r})] + \sum_{i<j} \phi_{\text{eff}}(\mathbf{R}_i, \mathbf{R}_j) \tag{1}$$

where the $\mathbf{p}_i$ are the momenta of the ions with masses m_i, U_0 is the structure-independent energy, and $\phi_{\text{eff}}(\mathbf{R}_i, \mathbf{R}_j)$ is the effective pair potential between ions i and j. The electron distribution is $n_e(\mathbf{r})$ and the positive reference jellium distribution is $\rho_0(\mathbf{r})$. In the work of Gryko and Rice[6] it was assumed, for the purpose of calculating the pseudopotential, that local electroneutrality prevailed in the liquid–vapor interface, i.e., $n_e(\mathbf{r}) = \rho_0(\mathbf{r})$ everywhere. In this work we use density functional theory to compute the electronic structure of the reference jellium as described in I. In this section we describe the calculations needed to compute the potential energy in Eq. (1), with attention paid to those aspects peculiar to the case of the liquid binary alloy. In our discussion, we use atomic units of length (1 au = 0.529177 Å, the Bohr radius) and energy (1 au = 27.116 eV = 2 Ry). It is frequently convenient to replace the density with the volume per atom, which we denote by Ω.

The pair potentials $\phi_{\text{eff}}(\mathbf{R}_i, \mathbf{R}_j)$ are calculated using the local density approximation expression

$$\phi_{\text{eff}}(\mathbf{R}_i, \mathbf{R}_j) = \phi_H(|\mathbf{R}_i - \mathbf{R}_j|; \tfrac{1}{2}[n_e(\mathbf{R}_i) + n_e(\mathbf{R}_j); i, j]) \tag{2}$$

$\phi_H(R, \rho; i, j)$ is the pair potential between two ions i and j separated by a distance R in a homogeneous fluid of density ρ, and is given for alloys by

$$\frac{\bar{Z}_i \bar{Z}_j}{R}\left\{1 - \frac{1}{\pi}\int_0^\infty dq\,[F_{i,j}(q) + F_{j,i}(q)]\,q^{-1}\sin(Rq)\right\} + BM(R) + vw(R) \tag{3}$$

where the first term includes the electron–ion pseudopotential effects as derived by Wang and Lai,[7] and the last two terms are small corrections for the Born–Mayer core–core repulsion[8] and the van der Waals core polarization interactions, respectively.[9,10] In Eq. (3), $\bar{Z}_i$ and $\bar{Z}_j$ are the effective valences of the two ions. Their product, $\bar{Z}_i\bar{Z}_j$, is $Z_iZ_j - \rho_{d_i}\rho_{d_j}$, where the ρ_d are the depletion hole charges of the ions and the Z's are the real valences. The $F_{i,j}(q)$ are the energy characteristic wave numbers. The

explicit usage of the subscripts i and j in the formula indicates that the interactions depend on whether both ions are cesium, both are sodium, or one is sodium and the other cesium. Both $F(q)$ and ρ_d are dependent on the electron density and the composition of the alloy; they are computed using the self-consistent pseudopotential formalism and method of Woo *et al.*[11] as extended to binary alloys by Wang *et al.*[12] In each simulation, we ignore the effect of the differences in the composition of various layers of the interface on the energy characteristic wavenumbers and the depletion hole charges used in computing the pair potentials; for a given pair of ions, we use the pair potential for a homogeneous fluid of the bulk composition whose electron density is given by the local density approximation of Eq. (2). As in I, we cut off the effective pair potential at 19 au and ignore its density dependence at densities below about one-third of the bulk density of the alloy being simulated. The tabulation and interpolation of ϕ_H as a function of R and n_e are carried out as described in I, but now tables must be drawn up for each of the three types of interactions, Na–Na, Na–Cs, and Cs–Cs. When a given ion is moved, we use the standard formula to account for the change in the interactions involving that particular ion and the method described in I to account for the change in the interaction between all other pairs of particles due to the change in the electron distribution caused by the movement of the particles.

All simulations are performed on a slab of ions with a free surface. For each configuration of ions a slablike reference jellium must be determined in order to evaluate the potential energy in the Hamiltonian (1). We assume that the density distribution of this jellium has the functional form

$$\rho_0(z; z_0, \beta) = \frac{\rho_b}{1 + \exp[(|z| - z_0)/\beta]} \tag{4}$$

where the variable parameters β and z_0 are determined for each configuration by a weighted least squares fit of the discrete moments of the ion distribution to the continuous moments of $\rho_0(z; z_0, \beta)$, requiring $\rho_b = N_T/2A$ to ensure that the jellium distribution is properly normalized. N_T is the total number of particles and A is the area in the xy plane of one face of the slab. The Gibbs dividing surface is located at z_0 and the 10%–90% width of the profile is 4.4β. The details of this fitting procedure are described in I.

The determination of the electronic structure and the structure-independent energy have already been described in I. We use the density functional theory instead of the local electroneutrality approximation for the electronic structure in all calculations described in this paper. The only modification to the formalism in I is the generalization of the per-particle pseudopotential contribution to the structure-independent energy ε_{ps} from

the special case of a one-component system to that of a binary alloy. We use the formula presented in Ref. 6,

$$\varepsilon_{ps} = 3\int_0^1 d\eta\, \eta^2 f(\eta,\eta) - \frac{2\pi}{\Omega_0}\sum_{i=1}^{2}\sum_{j=1}^{2}\bar{Z}_i\bar{Z}_j X_i X_j \lim_{q\to 0}\frac{1-F_{i,j}(q)}{q^2}$$
$$-\frac{1}{\pi}\sum_{i=1}^{2} X_i\int_0^\infty dq\,[\rho_{d_i}^2 |M_i(q)|^2 + \bar{Z}_i^2 F_{i,i}(q)] + \left(\frac{\alpha}{r_s}+\frac{\beta}{r_s^2}\right) \tag{5}$$

in which the $f(\eta,\eta)$ are the diagonal elements of the non-Columbic part of the pseudopotential for $k=\eta k_F$, where k_F is the Fermi wave vector, the $M_i(q)$ are the Fourier transforms of the depletion hole densities, and X_i is the mole fraction of the ith component. The final two terms are the semiempirical corrections to the pseudopotential whose coefficients, α and β, are adjusted so that the bulk liquid metal has the proper heat of sublimation and is mechanically stable at its experimental density at 100°C. The total contribution of the electron–ion pseudopotential to the structure independent energy of the slab is

$$E_{ps} = 2A\int_0^\infty dz\,\rho_0(z)\,\varepsilon_{ps}(n_e(z)) \tag{6}$$

where throughout the interface the composition assumed in computing $\varepsilon_{ps}(n_e)$ from Eq. (5) is that of the bulk alloy.

3. SIMULATION TECHNIQUES

We have carried out Monte Carlo simulations using the scheme of Metropolis *et al.*[13] for three different sodium–cesium alloys at 100°C: $X_{Cs}=0.25$, 0.50, and 0.75, where X is the mole fraction. All of our systems are 1000-ion slabs with initial dimensions $L_0^*\times L_0^*\times 2L_0^*$, with periodic boundary conditions in the x and y directions and with free surfaces on both halves of the slab in the z direction. L_0^* is chosen so that the initial density of the slab is the experimental value, ρ_b^*. The simulation is started by placing the ions within the initial slab with a uniform random distribution and using a force bias Monte Carlo simulation to eliminate overlaps between ion cores, as described in I.

During the simulations ions are moved sequentially, and the moves are accepted or reject according to the Metropolis criterion. A pass is the movement of every particle once. To be sure that we sample only equilibrium configurations of the ions, we omit the first six to seven million configurations of each simulation in computing the properties of the system. The various properties of the system are calculated as described in I. The coordinate system is chosen so that the first moment of the ion distribution (the center of mass when all ions have equal masses) is fixed at zero in the z direction. Density profiles from each half of the slab are

Table I. Summary of Simulation Characteristics[a]

Substance	ρ_b^{*-1} (au^3)	$\langle \rho_b \rangle^{-1}$ (au^3)	N_R $\times 10^6$	N_C $\times 10^6$	L_S (au)	P_A	L_0^* (au)
Pure Cs[b]	830	780	2.9	6.8	1.50	59	74.59
25% Cs alloy	395	369	6.0	16.0	1.58	42	58.23
50% Cs alloy	523	471	6.0	7.2	1.00	55	63.97
75% Cs alloy	669	646	6.0	12.4	1.38	58	69.41
Van der Waals analog of 50% Cs alloy	—	726	7.2	3.2	1.00	60	63.97

[a] N_R is the number of initial configurations rejected, in millions. N_C is the number of configurations used in collecting statistics, in millions. L_S is the step size used, in au. P_A is the percentage of moves accepted by the Metropolis algorithm.

[b] This cesium simulation is the one without the local electroneutrality approximation discussed in I.

averaged together. Pair correlation functions are calculated for only the $z > 0$ half of the slabs, except for the case of the 50% Cs alloy, for which values from strata on opposite sides of the slab are averaged together. The slices used in this discussion are taken at $0.0 < z < 0.4L_0^*$, $0.7L_0^* < z < 0.8L_0^*$, $0.8L_0^* < z < 0.9L_0^*$, and $0.9L_0^* < z < 1.0L_0^*$, where L_0^* is defined above. The reader should keep in mind that the edge of the slab is at $z < L_0^*$ because the average densities of the slabs turned out to be higher than the experimental densities by about 5–10%. A summary of the parameters used in the simulation and some of our results are shown in Table I.

4. RESULTS

In general, the convergence of a Monte Carlo simulation of an inhomogeneous alloy is much slower than the corresponding simulation of a pure metal. In particular, it is necessary to carry out enough iterations of the procedure before collecting statistics that the compositions in different layers can equilibrate. As can be seen in Table I, the simulations predict bulk densities that are higher than the experimental values, even with the semiempirical corrections to the pseudopotential we have used. We attribute this error to a combination of finite-sample-size effects, the inaccuracy of the pseudopotential and the strong oscillations in the longitudinal density profile. For 50% Cs alloy the moment fitting procedure failed (gave $\beta < 0$). This failure was traced to the inability of the simple reference density form to fit the inhomogeneities encountered in the simulation.

Total ion longitudinal density profiles, Cs longitudinal density profiles. Na longitudinal density profiles, and Cs longitudinal concentration profiles for the liquid–vapor interface of each of the alloys we have studied are shown in Figs. 1–3. The simulations show that the liquid–vapor interfaces of these alloys can be described as a monolayer of pure cesium sitting on top of a slab of the bulk alloy. The width of the interface between this "monolayer" and the bulk alloy is less than one atomic diameter. When the cesium concentration is high, e.g., $X_{Cs} = 0.75$, the cesium component of the liquid–vapor interface of the alloy shows stratification resembling that of the liquid–vapor interface of pure cesium, whereas the sodium longitudinal density distribution is structureless within the accuracy of the simulation. The longitudinal density profiles of the 50% and the 25% cesium alloys show a slight excess of sodium in the layer adjacent to the cesium monolayer. This feature of the composition distribution appears very early

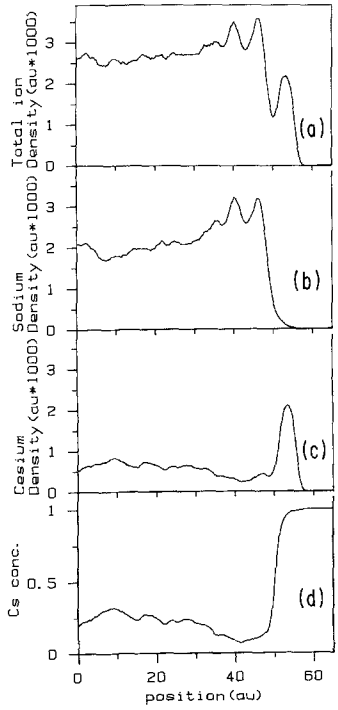

Fig. 1. Longitudinal density profiles of the slab of the 25% cesium alloy. (a) Total density, (b) sodium density, (c) cesium density, and (d) cesium concentration (in mole fraction).

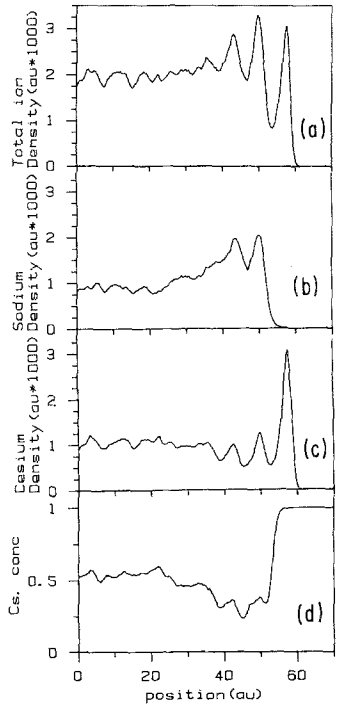

Fig. 2. Longitudinal density profiles of the slab of the 50% cesium alloy. (a) Total density, (b) sodium density, (c) cesium density, and (d) cesium concentration (in mole fraction).

in the simulations, within the first million configurations, and persists throughout the entire length of the simulation; its significance is discussed below.

Is the tendency of the cesium to form a well-defined monolayer at the liquid–vapor interface of the alloy a characteristic peculiar to liquid metals? Monte Carlo and molecular dynamics simulations of the liquid–vapor interface of a van der Waals binary liquid mixture of particles interacting with Lennard-Jones potentials suggest that this is the case.[14] In that van der Waals system the pair potentials for the two components differ only in the well depths, not the well positions (i.e., the components have the same effective diameters as defined by Barker–Henderson perturbation theory). The simulations of this system predict monotonic longitudinal density

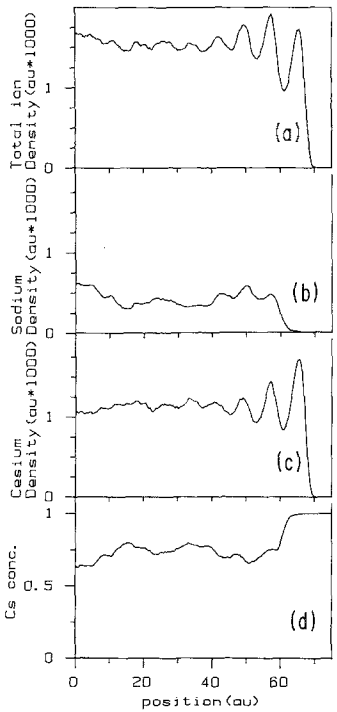

Fig. 3. Longitudinal density profiles of the slab of the 75% cesium alloy. (a) Total density, (b) sodium density, (c) cesium density, and (d) cesium concentration (in mole fraction).

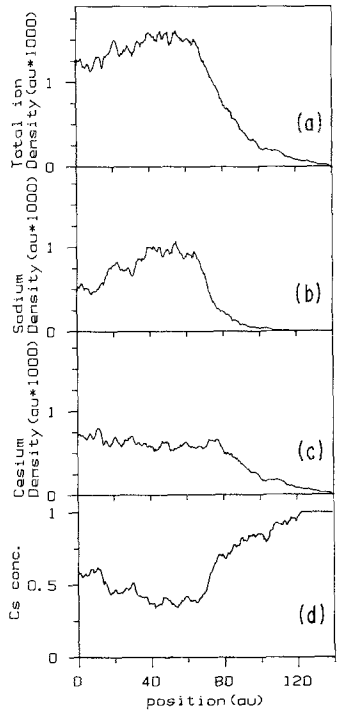

Fig. 4. Longitudinal density profiles of the slab of the pseudo-van der Waals analog of the 50% cesium alloy. (a) Total density, (b) density of the sodiumlike component, (c) density of the cesiumlike component, (d) concentration of the cesiumlike component (in mole fraction).

profiles for both components, and a gradual monotonic increase in the concentration of the component with the lower vapor pressure, going from the liquid to the vapor side of the interface.

Aside from its metallic character, our system differs from that of the previously cited work in that the sodium and cesium have very different effective diameters (6.3 and 9.3 au, respectively, using the inner zero of the pair potential as the effective diameter). To identify the features of our interfacial longitudinal density profiles that are characteristic of metallic alloys, we simulated a van der Waals analog of the $X_{Cs} = 0.50$, $X_{Na} = 0.50$ alloy by neglecting the structure-independent energy and the density dependence of the pair potential. We used the effective pair potentials for the experimental density ($\Omega = 523$ au) for the three types of pair interactions and one of the later configurations from the simulation of the 50% cesium alloy as the starting configuration for this simulation. The density and concentration profiles predicted by this simulation are shown in Fig. 4. Because the structure-independent energy forms a large portion of the binding energy of the metal system, the equilibrium density of this pseudo-van der Waals system is much lower than that of the corresponding liquid metal. The structure of the liquid–vapor interface of this mixture is predicted to be very different from that of the alloy. As in the simulation of the previously mentioned Lennard-Jones system, the longitudinal density profiles for both components are broad and monotonic. The sodium longitudinal density profile still shows the broad hump beneath the interface. Simulations of this pseudo-van der Waals system at a lower temperature (50°C) show similar structure with a narrower liquid–vapor interface, a larger amount of sodium accumulating in the hump, and, consequently, a greater depletion of sodium from the center of the slab. These results lead us to conclude that the presence of the pure cesium monolayer on the outer side of the liquid–vapor interface is a feature peculiar to the liquid metal, while the hump in the longitudinal sodium profile in the interface is an effect of the differences in ion core sizes.

To show that the monolayer of cesium on the vapor side of the interface and the rapid change in concentration are not artifacts of the length of the simulation, we show in Figs. 5–7 cesium and sodium density and concentration profiles normal to the interface for consecutive sets of about six million configurations for the simulations of the 25% cesium alloy and the 75% cesium alloy. The features of the 75% cesium alloy remain almost unchanged, although the fluctuations in the sodium density profile increase slightly. Both systems also show a slight increase in the density oscillations of the cesium longitudinal density profiles, even deep into the slab. The density oscillations appear to propagate inward from the surface during the simulation, and they show the effect of the finite size of the slab used in our simulation. Because of the one-body term in the pseudopotential, the sur-

face tension is much greater in liquid metals than in van der Waals liquids, and its effects can therefore penetrate deeper into the slab. The propagation of the force derived from the gradient of the one-body potential from the surfaces on opposite halves of the slab produces slight density oscillations in the longitudinal density profile throughout the system. Whereas a 1000-atom slab of a Lennard-Jones fluid appears to be large enough to eliminate the finite-size effect to within the statistical error of the simulation, it appears that a 1000-atom slab of a liquid metal is not. Such finite-size effects can also be seen in simulations of van der Waals systems where the fluid is constrained between two walls.

The later 6.4 million configurations of the 25% cesium alloy show a slight decrease in the size of the hump in the sodium density. An examination of intermediate longitudinal density profiles from groups of 800,000 configurations shows that this trend ends in the middle of this

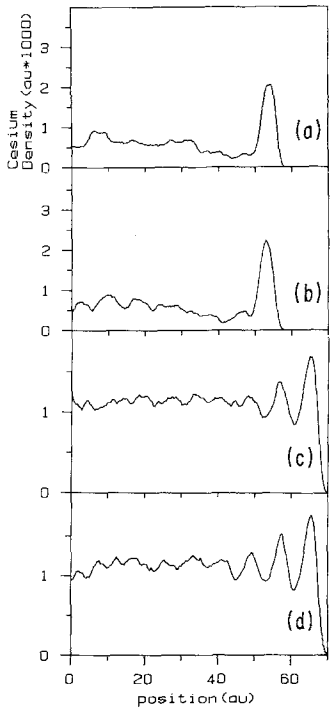

Fig. 5. Longitudinal cesium density profiles from (a) 6400 passes starting at pass 6003 of the 25% cesium alloy, (b) 6400 passes starting at pass 12,403 of the 25% cesium alloy, (c) 6400 passes starting at pass 6013 of the 75% cesium alloy, (d) 6000 passes starting at pass 12,413 of the 75% cesium alloy.

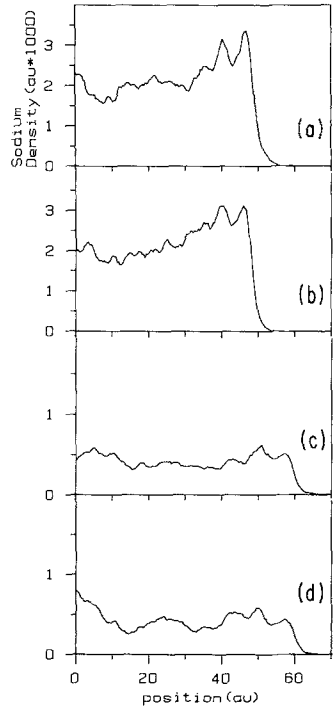

Fig. 6. Longitudinal sodium density profiles from (a) 6400 passes starting at pass 6003 of the 25% cesium alloy, (b) 6400 passes starting at pass 12,403 of the 25% cesium alloy, (c) 6400 passes starting at pass 6013 of the 75% cesium alloy, (d) 6000 passes starting at pass 12,413 of the 75% cesium alloy.

group of configurations, and the number of sodium atoms in the region $0.7L_0^* < z < 0.9L_0^*$, which is in the hump, see Table II, begins to increase after about 16,000 passes. Because the large Cs ions diffuse slowly in this alloy, we are reluctant to assert that this feature of the system is real and not a transient fluctuation which has not disappeared in the time available for computation. On the other hand, the likelihood that this is a real feature of the system is further supported by its persistence in the simulations of the pseudo-van der Waals analog of the 50% cesium alloy, and the decrease in the amount of the sodiumlike component in the center of the slab when the temperature is lowered.

The lack of structure in the transverse density profiles, taken from a region of $0.4 \times L_0^*$ on either side of the center of the slab and shown in

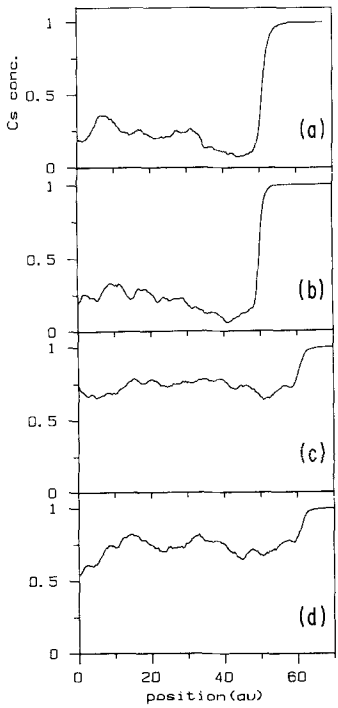

Fig. 7. Longitudinal cesium concentration (in mole fraction) profiles from (a) 6400 passes starting at pass 6003 of the 25% cesium alloy, (b) 6400 passes starting at pass 12,403 of the 25% cesium alloy, (c) 6400 passes starting at pass 6013 of the 75% cesium alloy, (d) 6000 passes starting at pass 12,413 of the 75% cesium alloy.

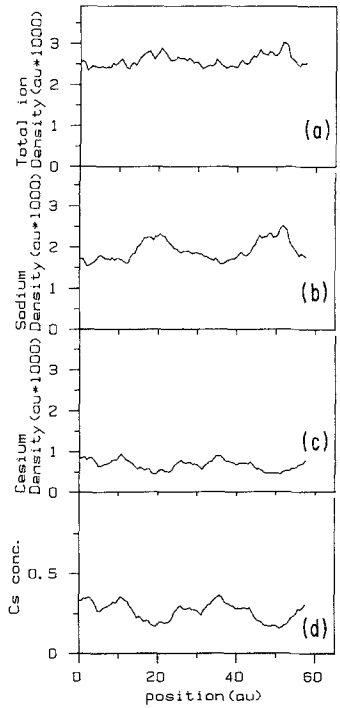

Fig. 8. Transverse density profiles from around the center of the slab of the 25% cesium alloy. (a) Total density, (b) sodium density, (c) cesium density, (d) cesium concentration (in mole fraction).

Figs. 8–10, indicates that the features we observe in the longitudinal density distribution are characteristic of the liquid–vapor interface structures and not due to the formation of a glassy or crystalline state. Their roughness shows approximately the amount of noise for the simulations.

Sodium–sodium, sodium–cesium, and cesium–cesium pair correlation functions taken from several layers of the 75% and 25% cesium alloys are shown in Figs. 11 and 12, and the positions of these layers are shown in Table II. Because both composition and density change throughout the interface, an analysis of the pair correlation functions is not as simple and straightforward as for the pure liquid metal. In I we examined the transverse pair correlation function in interfacial strata cut parallel to the surface and found that the position of the outermost peak of that function moves to greater R as the location of the stratum moves from the liquid to

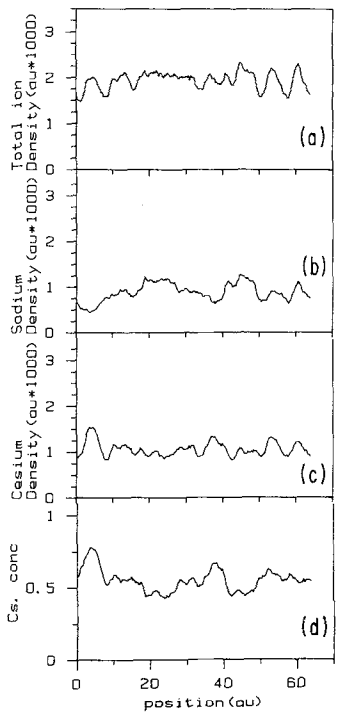

Fig. 9. Transverse density profiles from around the center of the slab of the 50% cesium alloy. (a) Total density, (b) sodium density, (c) cesium density, (d) cesium concentration (in mole fraction).

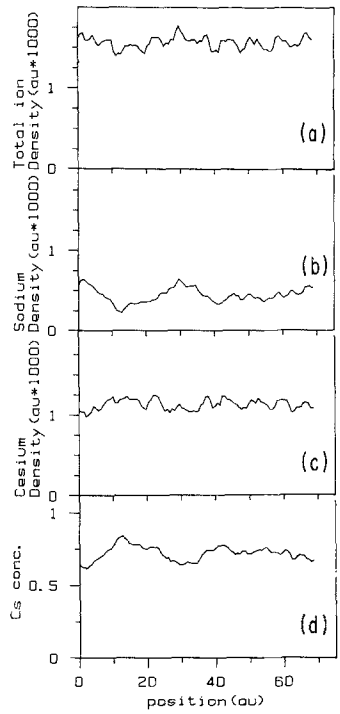

Fig. 10. Transverse density profiles from around the center of the slab of the 75% cesium alloy. (a) Total density, (b) sodium density, (c) cesium density, (d) cesium concentration (in mole fraction).

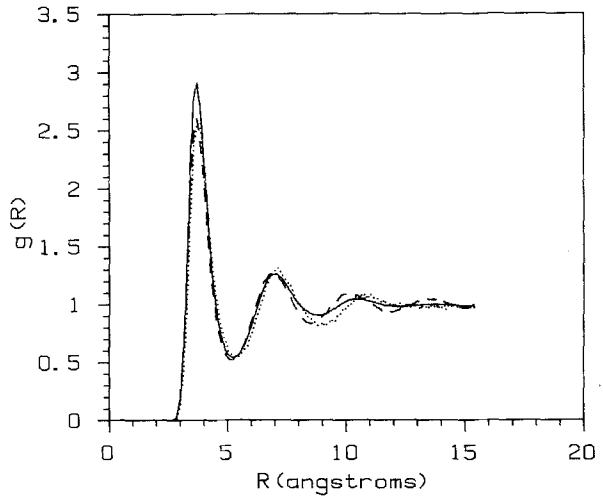

(a)

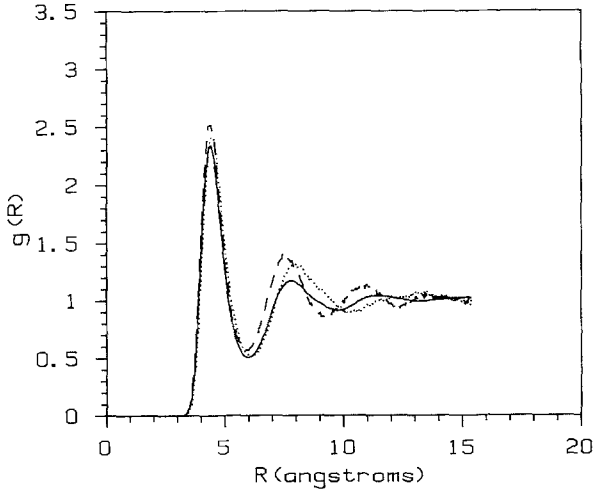

(b)

Fig. 11. Transverse pair correlation functions of the layers (—) $0.0 < z < 0.4L_0^*$, (- -) $0.7L_0^* < z < 0.8L_0^*$, (···) $0.8L_0^* < z < 0.9L_0^*$, (- - -*) and $0.9L_0^* < z < 1.0L_0^*$ from the 25% Cs alloy slab. (a) Na–Na pair correlation functions, (b) Na–Cs pair correlation functions, and (c) Cs–Cs pair correlation functions. The layer $0.9L_0^* < z < 1.0L_0^*$ has only cesium present, and the asterisks are at only a few selected data points for the purpose of clarity.

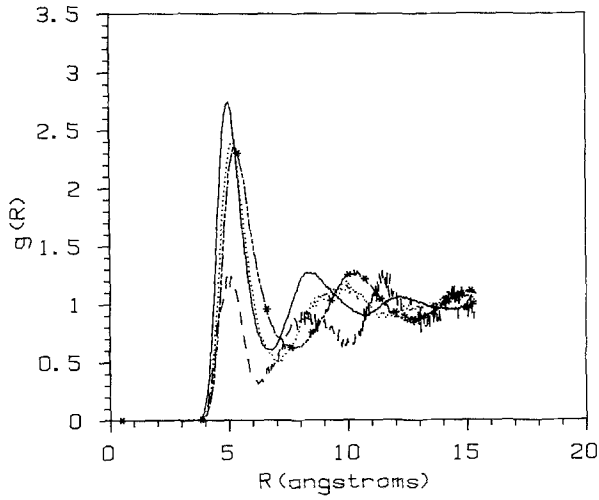

(c)

Fig. 11 (*continued*)

the vapor side of the interface. This shift is characteristic of the almost monotonic decrease from the liquid to the vapor side of the interface in the "nominal density," defined for each location as the point density averaged over the volume of an atomic-sized sphere centered at it. We have shown elsewhere that this nominal density is an accurate predictor of the pair correlation function beyond its innermost peak.[15] Because each of the three types of pair correlation functions are influenced by the same excluded-volume effects, the cesium–cesium, cesium–sodium, and sodium–sodium pair correlation functions behave similarly to each other. In the 25% and 50% alloys, the phases of the outer peaks of the pair correlation functions taken from $0.7L_0^* < z < 0.8L_0^*$ are shifted inward compared with the pair correlation functions taken from $0.0 < z < 0.4L_0^*$, contrary to what was seen in simulations of a pure liquid metal. This pattern is strongest in the cesium–sodium pair correlation function. It is consistent with the observation that the local density near the center of the slab is slightly lower than the local density beneath the cesium monolayer for these two alloys.

For each alloy the outermost layer of the liquid–vapor interface has the same composition—pure cesium. As can be seen in Fig. 12, transverse pair correlation functions taken from this cesium stratum in each alloy are almost identical to the transverse pair correlation function in the outermost peak of the pure cesium simulation, except for the height of the nearest

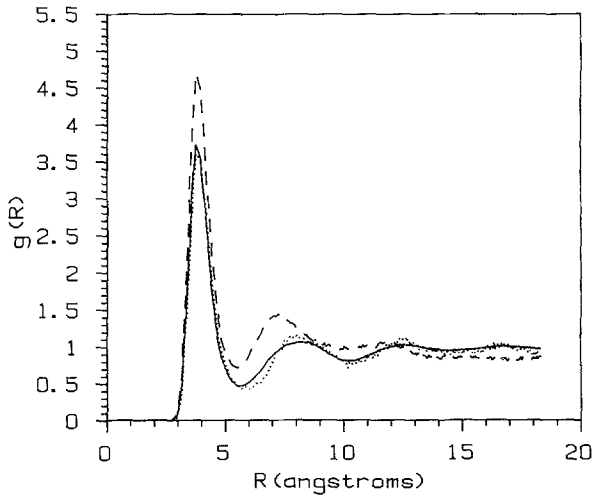

(a)

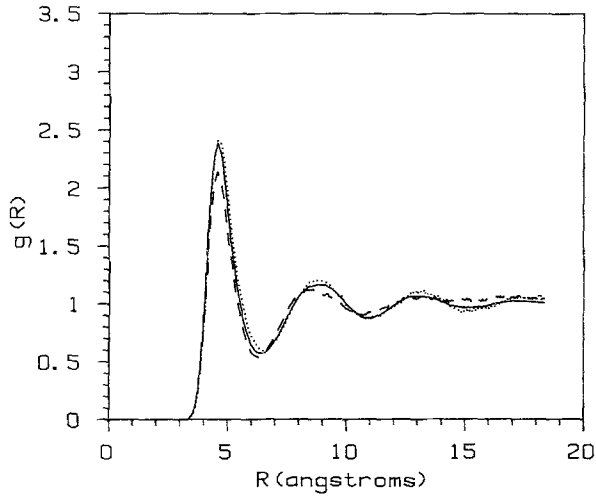

(b)

Fig. 12. Transverse pair correlation functions of the layers (—) $0.0 < z < 0.4L_0^*$, (- -) $0.7L_0^* < z < 0.8L_0^*$, (···) $0.8L_0^* < z < 0.9L_0^*$, (- - -*) and $0.9L_0^* < z < 1.0L_0^*$ from the 75% Cs alloy slab. (a) Na–Na pair correlation functions, (b) Na–Cs pair correlation functions, and (c) Cs–Cs pair correlation functions. The layer $0.9L_0^* < z < 1.0L_0^*$ has only cesium present, and the asterisks are at only a few selected data points for the purpose of clarity.

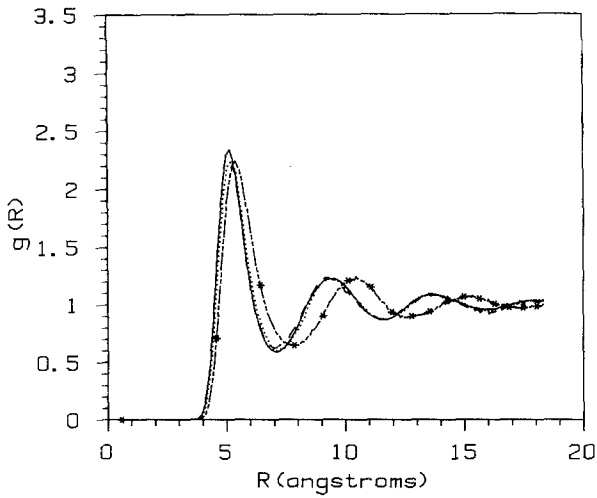

(c)

Fig. 12 (*continued*)

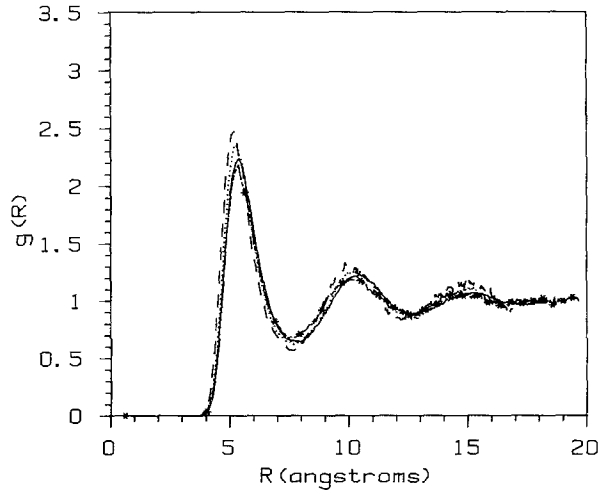

Fig. 13. Cesium–Cesium transverse pair correlation functions of the cesium monolayer ($0.9L_0^* < z < 1.0L_0^*$) for (- - -*) slabs of pure cesium, (—) the 75% cesium alloy, (- -) the 50% cesium alloy, and (···) the 25% cesium alloy.

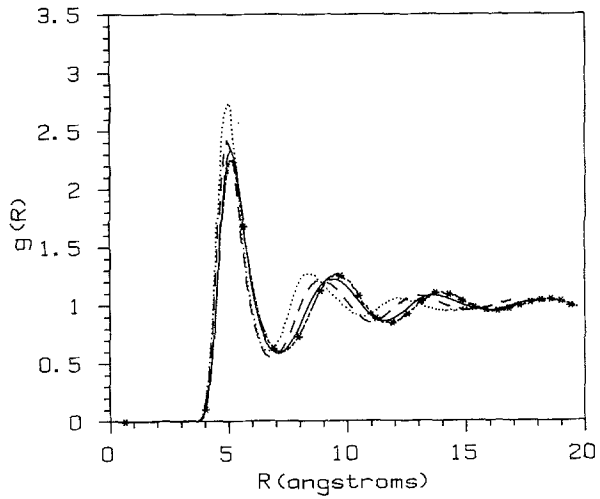

Fig. 14. Cesium–cesium transverse pair correlation functions of the bulk ($0.0 < z < 0.4L_0^*$) from (- - -*) slabs of pure cesium, (—) the 75% cesium alloy, (- -) the 50% cesium alloy, and (···) the 25% cesium alloy.

neighbor peak. The nearest neighbor peak height seems to be determined by the maximum local density of the monolayer, being largest in the case of the 50% cesium alloy, for which the outer cesium peak in the longitudinal density profile is highest, and smallest for the pure cesium slab, for which the corresponding maximum in the density profile is lowest. The nearest neighbor peak heights of the pair correlation functions from the strata of pure cesium in the other alloys also follow this pattern. The similarity in these cesium–cesium pair correlation functions is to be contrasted with the differences between the pair correlation functions taken from the centers of the slabs, shown in Fig. 13. The latter show the expected outward shift of the outer peaks of the pair correlation function in the lower density alloys.

5. DISCUSSION

The longitudinal density profiles predicted by our simulations of the liquid–vapor interfaces of NaCs alloys show that the structure-independent energy of the liquid metal has a strong influence on the surface composition. We expect that in a mixture the component with the larger atomic diameter will segregate toward the vapor side of the interface so as to maximize the space available to the large particles. In the liquid–vapor interface of a van der Waals fluid, the longitudinal density profile spreads over two to three atomic diameters, so the packing is not much constrained. In the liquid metal, whatever atoms are present at the surface are

forced to lie within a narrow stratum by the force derived from the structure-independent energy. To minimize the energy increase due to broken pair interactions, these particles must be the ones that are larger and have the weaker pair interactions. Ions beneath this layer can have interactions with all of their nearest neighbors. Hence, except in the outermost layer, the energetic and entropic advantage of compositions different from the bulk concentration is small.

The reader should note that we have not included the possibility that the variation of the structure-independent energy through the interface will serve as a driving force for the segregation of the components of the alloy. That is, we have assumed that the sodium and cesium ions feel the same decrease in their self-energy from the electron–ion pseudopotential in going from the liquid to the vapor side of the interface, and that the effect of the segregation on the electronic structure of the interface is insignificant. Since sodium has the lower vapor pressure and the larger self-energy, we expect the inclusion of such an effect can only increase the degree of surface segregation of Cs, which is already sensibly complete.

For systems in which both components have similar core sizes and/or different valences, the effect of the self-energy of the ions and the change in the electronic structure on the interface structure could become important. The inclusion of such features in the pseudopotential formalism would likely involve fitting each ion distribution to a reference jellium, such as that shown in Eq. (4), and computing electronic structures and structure-independent energies as functions of the four parameters obtained from such a fit. Such an approach would still neglect the nonlocal nature of the ion self-energies, which arises because the self-screening results from the response of the global electron density to the presence of the ion. Foiles and Ashcroft[16] have shown that these nonlocal effects become significant in metals with high electron density and large valences.

The above suggestion for improving the treatment of the structure-independent energy would, of course, increase the computational effort involved in the simulations. Currently, for a typical NaCs alloy, one million configurations takes CPU 76.4 hr on a Celerity C1260, 37.5 CPU hr on an Elxsi Mod I processor, and 3.05 CPU hr on a Cray XMP/24.

ACKNOWLEDGMENTS

This research has been supported in part by NSF grant CHE 84-14012. Some of the computations in this work were carried out using the NCSA's Cray computing facility at Urbana, Illinois. Jonathan Harris was supported by the NSF Graduate Fellowship program and the McCormick Foundation while carrying out this research.

REFERENCES

1. F. F. Abraham, D. E. Schreiber, and J. A. Barker, *J. Chem. Phys.* **62**:1958 (1975).
2. M. P. D'Evelyn and S. A. Rice, *J. Chem. Phys.* **78**:5225 (1983).
3. M. P. D'Evelyn and S. A. Rice, *J. Chem. Phys.* **78**:5081 (1983).
4. J. G. Harris, J. Gryko, and S. A. Rice, *J. Chem. Phys.* **86**:1067 (1987).
5. J. W. Allen and S. A. Rice, *J. Chem. Phys.* **68**:5053 (1978).
6. Jan Gryko and S. A. Rice, *J. Chem. Phys.* **80**:6318 (1984).
7. S. Wang and S. K. Lai, *J. Phys. F* **10**:2717 (1980).
8. T. L. Gilbert, *J. Chem. Phys.* **49**:2640 (1968).
9. J. C. Upadhyaya, S. Wang, and R. A. Moore, *Can. J. Phys.* **58**:905 (1980).
10. J. J. Rehr, E. Zaremba, and W. Kohn, *Phys. Rev. B* **12**:2062 (1975).
11. C. H. Woo, S. Wang, and M. Matsuura, *J. Phys. F* **5**:1836 (1975).
12. S. Wang, S. K. Lai, and C. B. So, *J. Phys. F* **10**:445 (1980).
13. N. Metropolis, A. W. Rosenbluth, M. N. Rosenbluth, A. H. Teller, and E. Teller, *J. Chem. Phys.* **21**:1087 (1953).
14. G. A. Chapela, G. Saville, S. M. Thompson, and J. S. Rowlinson, *Chem. Soc. Faraday II* **73**:1133 (1977).
15. J. G. Harris, J. Gryko, and S. A. Rice, *J. Chem. Phys.* **86**:5731 (1987).
16. S. M. Foiles and N. W. Ashcroft, *Phys. Rev. A* **30**:3136 (1984).